# Supercharging a MnO₂ Nanowire: An Amine-Altered Morphology Retains Capacity at High Rates and Mass Loadings

Girija Thesma Chandran,[†] Gaurav Jha,[†] Shaopeng Qiao,[‡] Mya Le Thai,[†] Rajen Dutta,[‡] Alana F. Ogata,[†] Ji-Soo Jang,[¶] Il-Doo Kim,[¶] and Reginald M. Penner*[,†]

[†]Department of Chemistry and [‡]Department of Physics, University of California, Irvine, California 92697, United States
[¶]Department of Materials Science and Engineering, Korea Advanced Institute of Science and Technology (KAIST), 291 Daehak-ro, Yuseong-gu, Daejeon 34141, Republic of Korea
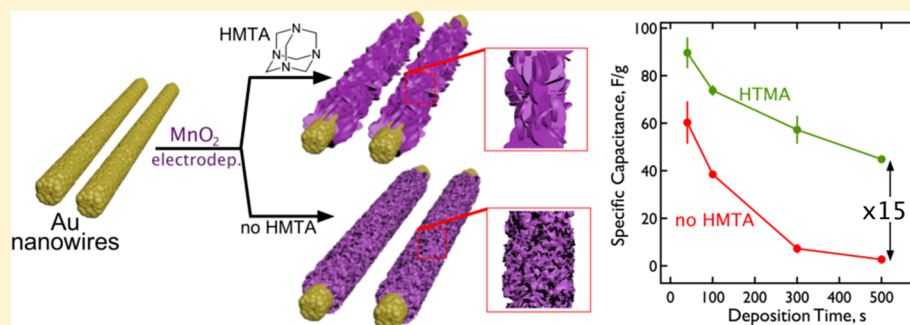
ABSTRACT: The influence of hexamethylenetetraamine (HMTA) on the morphology of δ-MnO₂ and its properties for electrical energy storage are investigated—specifically for ultrathick δ-MnO₂ layers in the micron scale. Planar arrays of gold@δ-MnO₂, core@shell nanowires, were prepared by electrodeposition with and without the HMTA and their electrochemical properties were evaluated. HMTA alters the MnO₂ in three ways: First, it creates a more open morphology for the MnO₂ coating, characterized by "petals" with a thickness of 6 to 9 nm, rather than much thinner δ-MnO₂ sheets seen in the absence of HMTA. Second, the electronic conductivity of the δ-MnO₂ is increased by an order of magnitude. Third, δ-MnO₂ prepared in HMTA shows a (001) interlayer spacing that is expanded by ≈30% possibly accelerating Li transport. The net effect of "HTMA doping" is to dramatically improve high rate performance, culminating in an increase in the specific capacity for the thickest MnO₂ shells examined here by a factor of 15 at 100 mV/s.

INTRODUCTION

Manganese oxide (Li$_x$MnO₂) is a Li⁺ insertion metal oxide with a high theoretical Faradaic charge storage capacity, C_{sp} of 1110 F/g (assuming a 1.0 V window), powered by Mn centers that can toggle between +2 or +3 oxidation states.[1−4] This Faradaic C_{sp} is higher than that for many insertion oxides including SnO₂ (640 F/g), RuO₂ (725 F/g), and Nb₂O₅ (726 F/g), and is comparable to Fe₂O₃ (1249 F/g) and Co₃O₄ (1206 F/g). C_{sp} values >1000 F/g are indeed measured experimentally in Li$_x$MnO₂ half-cells[5] and equivalent values of C_{sp} are seen in symmetrical Li$_x$MnO₂ capacitors,[6,7] but only for very slow charge/discharge rates in the 1−2 mV/s range and for very thin MnO₂ layers, with thicknesses <80 nm.[5] At higher rates, C_{sp} is rapidly reduced, by a factor of 10−50 at 100 mV/s, for example. C_{sp} is also depressed as the mass loading of MnO₂ on a current collector, and the shell thickness, increases. Thus, the tremendous potential of Li$_x$MnO₂ for energy storage in either capacitors or batteries is limited by poor rate performance, especially at significant mass loadings. These related phenomena are poorly understood at present.

What is the source of this poor rate performance? Barriers to Li⁺ intercalation/deintercalation at the MnO₂−electrolyte interface and slow Li diffusion within the MnO₂ are two contributing factors that have been proposed.[1,3,8] The influence of both of these mechanisms is minimized by increasing the level of dispersion of the MnO₂ by, for example, decreasing the MnO₂ particle diameter. Increased dispersion translates into a higher surface area:volume ratio and reduced diffusion path lengths within the MnO₂ for Li. A significant disadvantage of Li$_x$MnO₂—again shared by other metal oxides—is its low electronic conductivity which varies from 2 to 4 × 10⁻⁴ S/cm (x = 0) increasing to 4−5 × 10⁻² S/cm (for x = 1.0) as compared with ≈10⁵ S/cm for a metal such as silver.[9] The low conductivity of Li$_x$MnO₂ necessitates that it be supported at high dispersion on a good conductor such as a metal or carbon, and many examples of this general paradigm have been reported (e.g., refs 10−22). Our approach[5−7] has been to embed a gold nanowire within a shell of δ-MnO₂—so-called Au@δ-MnO₂ core@shell nanowires—where both the gold

nanowires and the δ-MnO$_2$ shell are prepared by electrodeposition. A key point is that the gold nanowire core does not ensure facile electrical communication with the MnO$_2$ shell when this shell increases in thickness beyond 60 nm or so. In Au@MnO$_2$ nanowires, the MnO$_2$ shell must still intercalate Li$^+$ and communicate electrically with the gold nanowire core, and the strategy outlined here is intended to impact one or both of these processes.

The well-known limitations of MnO$_2$ have stimulated interest in improving it, as already indicated. Hundreds of papers already describe the mitigation of the low electronic conductivity of MnO$_2$ by the preparation of composites of MnO$_2$ with graphene,[10−14] carbon nanotubes,[15−19] conductive polymers,[20−22] and other electrically conductive materials. In addition to the preparation of composites, there is some work aimed at altering the properties of the MnO$_2$ itself. Chen and co-workers[23] evaporated gold into MnO$_2$ films, thereby increasing the half-cell C_{sp} by a factor of 2 at 100 mV/s. This increase was attributed to the increased electrical conductivity of the MnO$_2$/Au composite. The MnO$_2$ morphology has been altered by hydrothermal synthesis in the presence of a surfactant, poly(vinylpyrrolidone) (PVP).[24] Single 40−50 nm diameter nanowires of MnO$_2$ with micron-scale lengths prepared by this technique showed a higher C_{sp} as compared with larger nanorods.[24] Nakayama and co-workers[25−27] prepared electrodeposited birnessite MnO$_2$ incorporating a variety of dopants including poly(diallyldimethyl-ammonium) cations,[25] methyl viologen,[26] and long chain, *n*-alkyl ammonium cations.[27] The *d*-spacing of the birnessite was adjusted over several nanometers by these dopant species, and applications of these composite materials to the catalysis of the oxygen evolution reaction were explored.[28]

Here we describe a process for altering the morphology of the electrodeposited MnO$_2$ shell using an amine dopant, hexamethylenetetraamine (HMTA)(Figure 1). Attention is
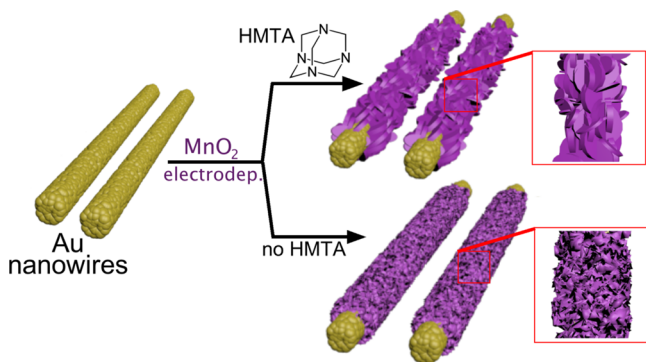
Figure 1. Schematic representation of the influence of HMTA on the morphology of Au@δ-MnO$_2$ nanowires prepared by electrodeposition. The properties of these two types of nanowires are compared in this paper.

focused on the properties of Au@δ-MnO$_2$ nanowires with thick MnO$_2$ shells (d_{MnO_2} = 400 nm to 2.2 μm) obtained using high MnO$_2$ mass loadings onto the gold nanowire. These nanowires exhibit a dramatic loss of C_{sp} (>95%) at high potential scan rates of 100 mV/s.[5−7] A more open morphology for the δ-MnO$_2$ is obtained in the presence of HMTA, in addition to two other observed changes: (1) the electronic conductivity of the δ-MnO$_2$ is increased by an order of magnitude, and (2) new reflections in the XRD pattern reveal

the (001) layer spacing increases significantly, possibly facilitating Li intercalaction/deintercalation and transport. HMTA gold@δ-MnO$_2$, core@shell nanowires show dramatically improved rate performance, characterized by an increase in C_{sp} of 15× at 100 mV/s for the thickest MnO$_2$ shells studied here.

■ MATERIALS AND METHODS

Chemicals and Materials. Manganese perchlorate hydrate, (Mn(ClO$_4$)$_2$·H$_2$O, 99%), lithium perchlorate (LiClO$_4$, battery grade, 99.99%), hexamethylenetetraamine (HTMA, 99.0%), iodine (I$_2$, 99.8%), and poly(methyl methacrylate) (PMMA, MW = 120 000 g/mol, 99.99%) were used as received from Sigma-Aldrich. Dry acetonitrile required for capacitance testing was prepared by processing reagent grade acetonitrile with a Jorg Meyer Phoenix SDS column purification system. Sulfuric acid (ULTREX ultrapure) was purchased from J. T. Baker. Potassium iodide (KI, 99%), acetone, propylene carbonate (PC, 99.7%), and nitric acid were used as received from Fisher (ACS Certified). Positive photoresists, Shipley S-1808 and developer MF-319 were purchased from Microchem Corporation. Nickel and gold pellets (5N purity, Kurt J. Lesker Co.) and chromium powder (3N purity, American Elements) were used for the preparation by thermal evaporation of ultrathin metal layers.

Preparation of Au@MnO$_2$ Core@Shell Nanowires. Au@MnO$_2$ core@shell nanowires were fabricated using a variant of the lithographically patterned nanowire electrodeposition (LPNE) technique shown schematically in Figure 2.[29−31] A 40 nm thick nickel film
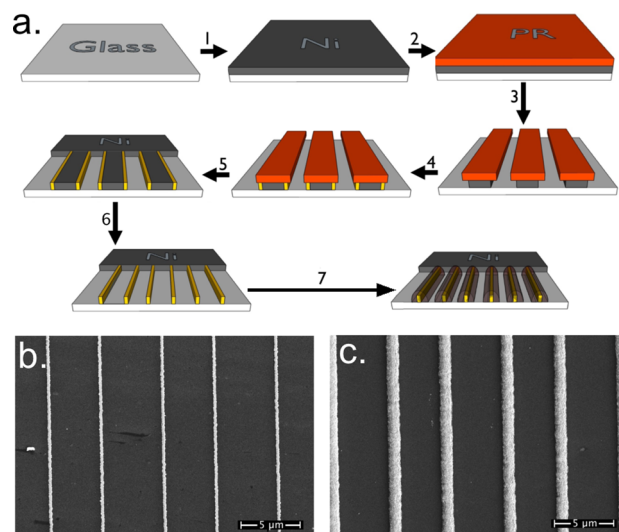
Figure 2. (a) Process flow for the preparation using lithographically patterned nanowire electrodeposition (LPNE) of Au@δ-MnO$_2$ nanowire arrays. (b) SEM image of five gold nanowires prepared using the process depicted above (steps 1−6). A typical array contained 1800 such nanowires. (c) Six Au@δ-MnO$_2$ nanowires prepared by the electrodeposition of δ-MnO$_2$ onto gold nanowires (step 7 above).

was first thermally evaporated on top of precleaned 1″ × 1″ squares of soda lime glass (Figure 2, step 1). Then a positive photoresist (PR, Shipley, S1808) layer was deposited by spin-coating (step 2), followed by soft-baking at 90 °C for 30 min, and a contact mask was used to pattern this PR layer with a 365 nm UV light source combined with a shutter and photolithographic alignment fixture (Newport, 83210i-line, 2.3s). The exposed PR region was developed for 20 s (Shipley, MF-319) and then rinsed with Millipore water (Milli-Q, ρ > 18 MΩ·cm). The exposed nickel was removed by etching for 6 min in 0.8 M nitric acid (step 3). The whole device was then dipped into commercial Au plating solution (Clean Earth Solutions), and Au was potentiostatically electrodeposited using a Gamry Series G 300
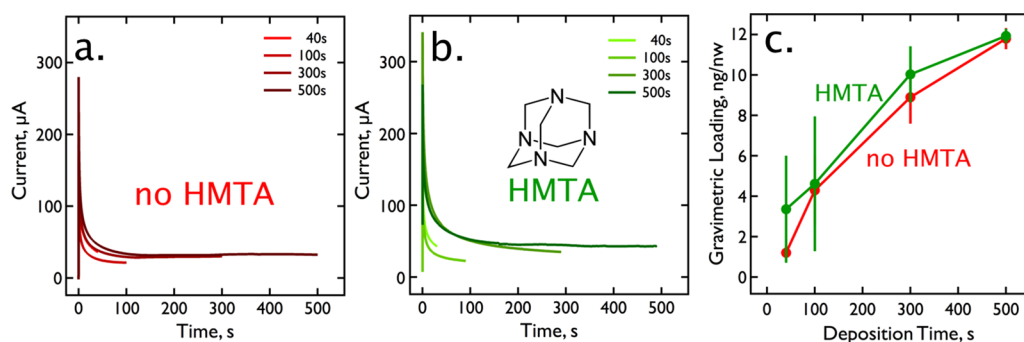
Figure 3. Electrodeposition of δ-MnO$_2$ onto a gold nanowire array. (a,b) Current versus time traces for the potentiostatic growth of δ-MnO$_2$ at +0.60 V vs MSE in solutions containing no-HMTA (a), and 10 mM HMTA (b), as described in the text. (c) Gravimetric loading of MnO$_2$ per nanowire (0.90 cm length) based upon the measured coulometry obtained from deposition data like that shown in panels a and b.

potentiostat at −0.9 V versus saturated calomel electrode (SCE) using a one-compartment, three-electrode electrochemical cell with a Pt foil counter electrode (step 4). After electrodeposition, the surface was first rinsed with acetone to remove photoresist, and then with Millipore water, revealing patterned Ni pads together with Au nanowires deposited on the edges of these pads (step 5). Nickel was then removed by immersion in nitric acid for 6 min (Step 6). After etching, the device was rinsed with Millipore water and air-dried. On the unetched side of this nanowire array, the Au nanowires still attached to nickel fingers were used as electrical contacts. This completes the preparation by LPNE of a gold nanowire array.

Finally, δ-MnO$_2$ was electrodeposited onto these nanowires (step 7) using either of two procedures: HMTA-free Au/MnO$_2$ nanowires were prepared using an aqueous solution of 2 mM Mn(ClO$_4$)$_2$ and 50 mM LiClO$_4$ by potentiostatic oxidation at +0.60 V vs MSE (saturated mercurous sulfate reference electrode), as previously described.[5] Deposition times ranging from 40 to 500 s produced MnO$_2$ shells between 400 nm and 2.2 μm in thickness. Au/MnO$_2$ core:shell nanowires containing HMTA were prepared using a two step procedure in which a thin HMTA-free "primer" layer was first electrodeposited as described above, using a t_{dep} = 10 s. Then, HMTA-doped δ-MnO$_2$ was electrodeposited onto MnO$_2$-primed gold nanowires from a solution containing 10 mM HMTA in addition to 2 mM Mn(ClO$_4$)$_2$ and 50 mM LiClO$_4$. t_{dep} ranging from 30 to 490 s resulted in the unique MnO$_2$ morphology described below. In both cases, freshly deposited Au@MnO$_2$ nanowires were removed from plating solutions, rinsed with Millipore water, and dried in the oven at 90 °C for 30 min prior to electrochemical assessment. All three-electrode, half-cell measurements were performed on arrays of 1800 nanowires. All capacitor measurements involved a sandwich of two 1800 nanowire layers.

Preparation of δ-MnO$_2$ Nanowire for Conductivity Measurements. "Solid" δ-MnO$_2$ nanowires, prepared without a Au core nanowire, were synthesized for conductivity measurements. These δ-MnO$_2$ nanowires were prepared following the LPNE method discussed in a previous work.[9] Although in this work electrodeposition of MnO$_2$ was carried out at a constant potential of +0.6 V vs MSE for 40, 100, 300, and 500 s using two different plating solutions, one with HMTA and one without HMTA, as discussed above.

Preparation of the Gel Electrolyte and Sandwich Capacitor Assembly. Symmetrical, Au@δ-MnO$_2$ nanowire "sandwich" capacitors were prepared by fabricating 1800 nanowire arrays on each of two glass substrates, and pressing these two layers together, using a ≈2 μm thick PMMA gel electrolyte, as previously described.[32] The 1.0 M LiClO$_4$, 20 w/w%, PMMA, PC gel electrolyte was prepared by adding 1.6 g (20 w/w%) of PMMA to 5 mL of 1.0 M LiClO$_4$ in dry propylene carbonate (PC) with mixing at 115 °C. In a desiccator, the mixed gel was permitted to cool to room temperature as it transformed to the gel state. The 1.0 M LiClO$_4$, 20 w/w%, PMMA, PC gel electrolyte was deposited on the device by spin-coating (2500 rpm, 160 s) resulting in a layer of ≈1 μm thickness. Two of these devices were combined to form a complete sandwich capacitor with a total PMMA gel layer

thickness of ≈2 μm. This assembly was accomplished by pressing together these nanowire layers with the electrical contacts oriented on opposite ends of the device. After assembly, sandwich capacitors were hermetically sealed to exclude moisture using hot glue prior to electrochemical characterization.

Structural Characterization. Scanning electron micrographs (SEMs) were acquired using a FEI Magellan 400 XHR system. Energy dispersive spectroscopic (EDS) images were acquired by the same SEM system with EDS detector (Oxford Instruments, 80 mm^2, with Aztec software). Accelerating voltages of incident electron beams ranged from 1 kV to 25 kV, and probe currents ranged from 13 pA to 0.8 nA. All SEM specimens were mounted on stainless stubs and held by carbon tape. Grazing-incidence X-ray diffraction (GIXRD) patterns were obtained using a Rigaku SmartLab X-ray diffractometer employing the parallel beam optics. The X-ray generator was operated at 40 kV and 44 mA with Cu Kα irradiation. X-ray photoelectron spectroscopy (XPS) was measured using the AXIS Supra by Kratos Analytical Inc. equipped with monochromatic Al/Ag X-ray source.

Electrochemical Characterization. All electrochemical measurements were performed in a one-compartment three-electrode cell using a Gamry potentiostat. The specific capacitance, C_{sp}, was measured in 1.0 M LiClO$_4$ in dry acetonitrile. Prior to each measurement, the acetonitrile was presaturated with N$_2$ gas. A Pt foil was used as a counter electrode in conduction with a saturated mercurous sulfate reference electrode (MSE). All potentials are quoted with respect to the saturated mercurous sulfate reference electrode (MSE), E_{MSE} = +0.640 V versus normal hydrogen electrode. A value of 0.78 μg/mC was used to determine MnO$_2$ shell masses from the deposition charge as required for the calculation of C_{sp}.[5]

■ RESULTS AND DISCUSSION

Electrodeposition of δ-MnO$_2$ From HMTA-Containing and HMTA-Free Plating Solutions. Linear arrays of 1800 gold nanowires with lateral dimensions of 275 nm (w) × 40 nm (h) were prepared on glass surfaces using the LPNE process (Figure 2a).[29−31] Gold nanowires were more than 1.0 cm in length, and were prepared with a wire-to-wire pitch of 5 μm (Figure 2b).

Au@δ-MnO$_2$ core@shell nanowires were obtained by exposing a 0.90 cm length of this array to a MnO$_2$ plating solution. δ-MnO$_2$ was electrodeposited in a hemicylindrical layer onto each of the gold nanowires in the array (Figure 2c). The same potentiostatic oxidation procedure was used for HMTA-containing plating solutions and HMTA-free solutions. This involved the electrochemical oxidation of Mn^{2+} at +0.60 V vs MSE:[6,7,9]

$$Mn^{2+} + 2H_2O \rightarrow MnO_2 + 4H^+ + 2e^- \tag{1}$$
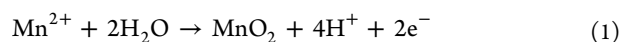
Table 1. Summary of Metrics for Au@δ-MnO₂ Prepared in HMTA-Containing and HMTA-Free Plating Solutions

δ-MnO₂	t_{dep}[a] (s)	thickness[b] (nm)	gravimetric loading[c] (ng/ nanowire)	C_{sp} (F/ g)	$C_{sp,HMTA}/$ $C_{sp,no-HMTA}$
no-HMTA	40	380 ± 80	1.2 ± 0.3	60 ± 9	
	100	660 ± 20	4.3 ± 2	39 ± 1	
	300	1080 ± 50	8.9 ± 1	7 ± 2	
	500	1800 ± 110	11.8 ± 0.5	3 ± 2	
HMTA	40	650 ± 20	3.4 ± 3	90 ± 6	1.5
	100	1070 ± 50	4.6 ± 3	74 ± 2	1.9
	300	1700 ± 50	10.0 ± 1	57 ± 6	8.1
	500	2200 ± 300	12 ± 0.4	45 ± 1	15

[a]The duration of the potentiostatic electrodeposition of MnO₂. [b]MnO₂ shell thickness measured using SEM. [c]Gravimetric loading is estimated from coulometry of the MnO₂ deposition. Loading pertains to nanowires 0.90 cm in length.
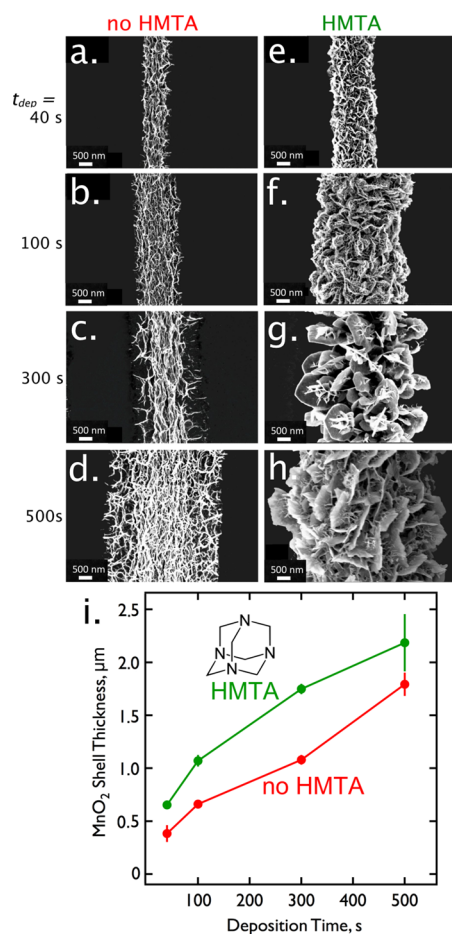
Figure 4. Influence of HMTA on morphology and apparent thickness of the δ-MnO₂ shell. (a−d) SEM images of Au@MnO₂ core@shell nanowires where the MnO₂ shell was prepared in the absence of HMTA. The deposition time, t_{dep}, is indicated at left. (e−h) Au/MnO₂ nanowires prepared in the presence of HMTA. (i) Plot of thickness of the MnO₂ shell outer envelope as a function of t_{dep}, based upon SEM images of these nanowires. The thickness of the shell envelope is one-half of the total width of the Au@δ-MnO₂ nanowires in plan-view SEM images like those shown in (a−h).

The unbuffered plating solution employed for this reaction had a pH = 7.2 ± 0.2 and the pK_a of HMTA is 4.9,[33] so it is unprotonated at this pH. The presence of 10 mM HMTA in the plating solution had a subtle influence on the kinetics of MnO₂ deposition, increasing the reaction rate by 2−5% as determined from current versus time traces (Figure 3a,b), but the gravimetric loading of MnO₂ per nanowire (Figure 3c), estimated from coulometry,[5] is the same within the reproducibility of the experiment (Table 1).
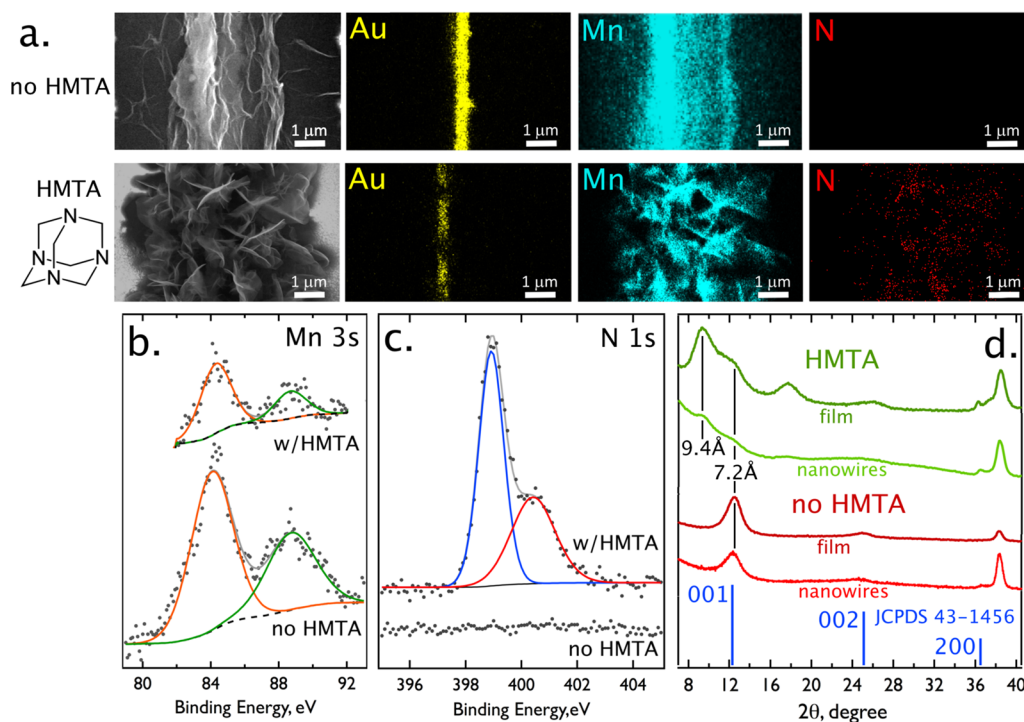
Characterization of Au@MnO₂ Core@shell Nanowires. As previously described,[6,7] the δ-MnO₂ shells obtained by electrodeposition from HMTA-free plating solution onto gold nanowires has a morphology that consists of many concentric, wrinkled MnO₂ sheets wrapped one on top of another (Figure 4a−d). In transmission electron microscopy (TEM) images, these sheets appear to have a thickness in the 2 nm range.[6] In the presence of 10 mM HMTA, in contrast, a more open structure is observed for the shell, characterized by MnO₂ "petals" radiating from the gold nanowire core. The apparent thickness of each MnO₂ petal, however, is much thicker in the 10−30 nm range depending upon the deposition duration (Figure 4,e-h). The "envelope" of the MnO₂ shell, plotted in Figure 4i, is also larger by 20−30% in spite of the fact that the Coulombic loading of MnO₂ per nanowire was approximately the same (Figure 3c).

This suggests that the porosity of the MnO₂ shell obtained in the presence of HMTA is greater than that which is obtained in its absence.

Electron dispersive X-ray analysis (EDX) elemental maps of single δ-MnO₂ nanowires (Figure 5a) show the presence of the central gold nanowire, and a manganese signal that spans the width of the δ-MnO₂ shell seen in the SEM image (Figure 5a, far left). Nitrogen is not detected for Au@δ-MnO₂ nanowires prepared in HMTA-free solutions, but is seen for those prepared in 10 mM HMTA solutions (Figure 5a, far right), with the nitrogen signal again spanning the width of the δ-MnO₂ shell seen in the SEM image. Based upon EDX survey spectra, nitrogen accounts for 5.4 (±0.40) at % in these samples.

XPS data were acquired for δ-MnO₂ films, prepared on platinum electrodes using the same deposition potential (+0.60 V vs MSE) employed for nanowire growth, and a 300 s deposition duration (Figure 5c,d). High resolution scans in the Mn 3s region (Figure 5b) show chemical shifts that are identical for δ-MnO₂ films prepared in the presence and absence of HMTA and characteristic of MnO₂ prepared at +0.60 V vs MSE.[7] For δ-MnO₂ films prepared from HMTA-free solutions, surface nitrogen is not detected in the N 1s region (Figure 5c), but it is seen in those δ-MnO₂ films prepared from HMTA-containing solutions at a surface concentration of 5.9 (±0.8) at %. Two distinct chemical shifts are observed for N 1s at 399.0 and 400.5 eV (Figure 5c). The 399.0 eV peak is characteristic of the sp³ nitrogens in HMTA.[34,35] A positive shift from this value might be expected upon protonation, but this is unlikely to be the case with HMTA because of the low pK_a of its nitrogens (4.9[33]). However, the incorporation of poly(aniline) into MnO₂[36] has been associated with the observation of N 1s binding energies in this range, possibly influenced by coordination to Mn centers. Based upon these observations, we tentatively assign the two peaks seen in the N 1s spectra to HMTA nitrogens that are perturbed by coordination to Mn centers (400.5 eV), and those that are not coordinated (399.0 eV).

For nanowires and films obtained with and without HMTA, grazing incidence X-ray powder diffraction (GIXRD) patterns for arrays of Au@δ-MnO₂ nanowires show weaker reflection

Figure 5. Characterization of Au@δ-MnO$_2$ nanowires (a,d) and δ-MnO$_2$ films (b,c,d). (a) EDX elemental maps of single of Au@δ-MnO$_2$ nanowires. An SEM image of the nanowire is shown at far left, and the elements mapped in each frame are as indicated. (b,c) XPS spectra of δ-MnO$_2$ films show high resolution scans in the Mn 3s region (b) and the N 1s region (c). (d) Grazing-incidence XRD (GIXRD) patterns are shown for both films and nanowires, as indicated. Reflections corresponding to the (001), (002), and (200) are observed in the patterns acquired for both HMTA and HMTA-free δ-MnO$_2$ sample. In addition, δ-MnO$_2$ prepared in 10 mM HMTA show two additional reflections at 9.6° and 18.5° that are assigned to first and second order diffraction from domains of δ-MnO$_2$ having an expanded interlayer spacing of ≈9.4 Å. An unlabeled XRD reflection at 37° is assigned to gold (111).
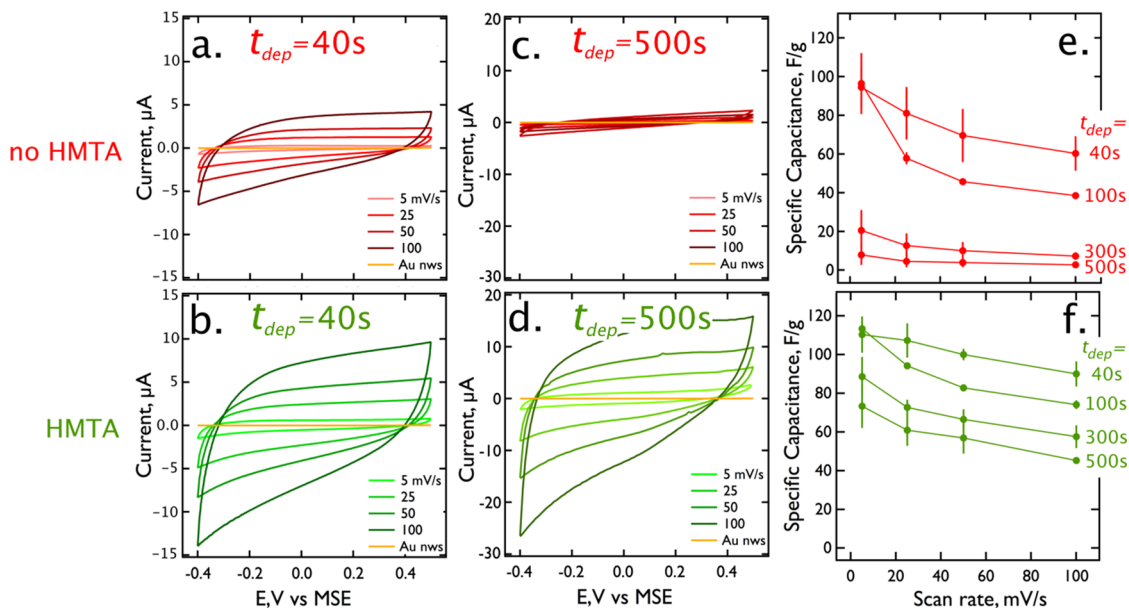
Figure 6. Cyclic voltammetry of no-HMTA and HMTA Au/MnO$_2$ core:shell nanowire arrays. (a,b) t_{dep} = 40 s corresponding to d_{MnO_2} = 600 nm (HMTA) and 400 nm (no-HMTA). (c,d) t_{dep} = 500 s corresponding to d_{MnO_2} = 2.2 μm (HMTA) and 1.8 μm (no-HMTA). Gold nanowires are cycled at 100 mV/s in all cases. (e,f) C_{sp} versus scan rate for both types of nanowires.

amplitudes than patterns acquired for films, but these patterns are otherwise very similar (Figure 5d). Films and nanowires prepared in the presence of HMTA show new reflections at 9.6° and 18.5° that we assign to first- and second-order diffraction from domains of δ-MnO$_2$ having an expanded interlayer spacing of ≈9.4 Å (Figure 5d). This is attributed to the inclusion of HMTA in the MnO$_2$ during growth. Weaker reflections at 12.2° and 24.5°, characteristic of δ-MnO$_2$ (JCPDS 43-1456), are still observed for these samples, but these
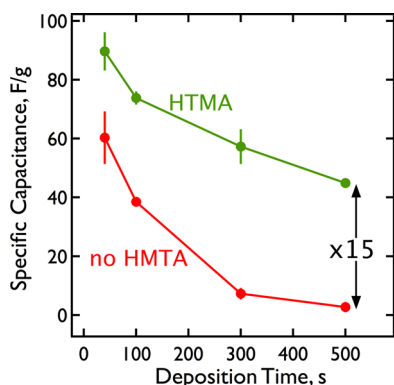
**Figure 7.** Comparison of C_{sp} at 100 mV/s for HMTA and no-HMTA Au@δ-MnO$_2$ nanowire arrays.

patterns are consistent with expansion of the interlayer spacing of δ-MnO$_2$ by $\approx$30% in the presence of HMTA.

The morphological, structural, and chemical changes induced in the δ-MnO$_2$ by HMTA, seen in the data of Figure 5, exert a strong influence on its electrochemistry particularly for very thick shells and high potential scan rates. For the thinnest shells studied here (t_{dep} = 40 s) evaluated at the slowest scan rates (5 mV/s), C_{sp} is 10% higher, on average, for HMTA versus no-HMTA samples (Figure 6a,b,e). This is a modest difference that is inside of our sample-to-sample error bars. The conclusion is that virtually the same number of Mn centers within these MnO$_2$ shells are electrochemically accessible and participating in Faradaic charge storage, thereby contributing to C_{sp}. It is important to understand that the C_{sp} = 90−110 F/g measured for these samples, with a shell thickness of 400−600 nm (Figure 4i), is well below the theoretical value of 1110 F/g.

C_{sp} values in this range are readily measured for arrays of Au@δ-MnO$_2$ nanowires with much thinner shells in the 60−70 nm range.[6,7]

However, as the scan rate is increased to 100 mV/s, even t_{dep} = 40 s nanowires show a clear disparity in C_{sp}, as seen by comparing the CVs shown in Figure 6a,b. For the thickest shells (t_{dep} = 500 s) at the highest scan rate (100 mV/s), the disparity between HMTA and no-HMTA samples is pronounced with C_{sp} 15× higher, on average, for HMTA versus no-HMTA samples (Figure 6c,d,e). The ability of δ-MnO$_2$ prepared in the presence of HMTA to store and deliver charge rapidly is significantly improved across all shell thicknesses examined here (Figure 7). The question is, why?

The increase in XRD (001) layer spacing induced by the electrodeposition of δ-MnO$_2$ in the presence of HMTA (Figure 5d) provides one rational. Accelerated Li transport between these expanded layers may be occurring. A second possible contributor to the improved rate behavior could be the electronic conductance of the δ-MnO$_2$. If the resistance of δ-MnO$_2$ shells prepared in HMTA was reduced, then the ohmic drop (IR) imposed by this shell at high scan rates would also be reduced, improving electrical communication across the radius of thick δ-MnO$_2$ shells. The conductance of "solid" δ-MnO$_2$ nanowires - that is, MnO$_2$ nanowires that contain no central gold nanowire - was measured in order to assess whether a significant difference in the electrical conductance was induced by the HMTA. Arrays of solid δ-MnO$_2$ nanowires were fabricated using LPNE as previously described (Figure 8a).[9] The morphology of HMTA and no-HMTA nanowires (Figure 8b,c) mimics that seen for Au@δ-MnO$_2$ nanowires (Figure 4a−h), but in contrast to Au@δ-MnO$_2$ nanowires, the lateral dimensions of the solid nanowires are controlled by the LPNE
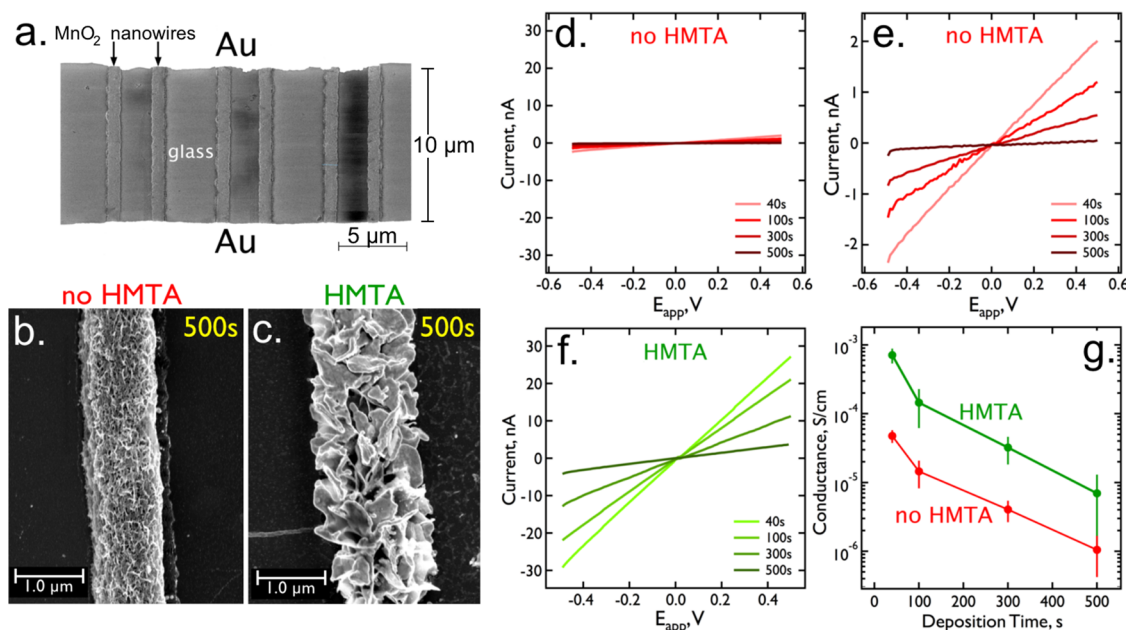
Figure 8. Measurement of MnO$_2$ nanowire conductance for no-HMTA and HMTA nanowires. (a) SEM image of six nanowires on glass. In this image, gold electrical contacts are located at the top and bottom of the image. (b,c) Higher magnification SEM images of HMTA (b) and no-HMTA (c) MnO$_2$ nanowires deposited for 500 s. These nanowires contain no central gold nanowire, enabling the measurement of the electrical conductance of the MnO$_2$. (d,e) Current versus voltage for a no-HMTA nanowire array at two current sensitivities, as indicated. (f) Current versus voltage for a HMTA nanowire array at at the same current sensitivity shown in (d). (g) Electrical conductance versus electrodeposition time for the four deposition times explored in this study. HMTA MnO$_2$ nanowires show a conductance approximately 1 order of magnitude higher than no-HMTA nanowires.
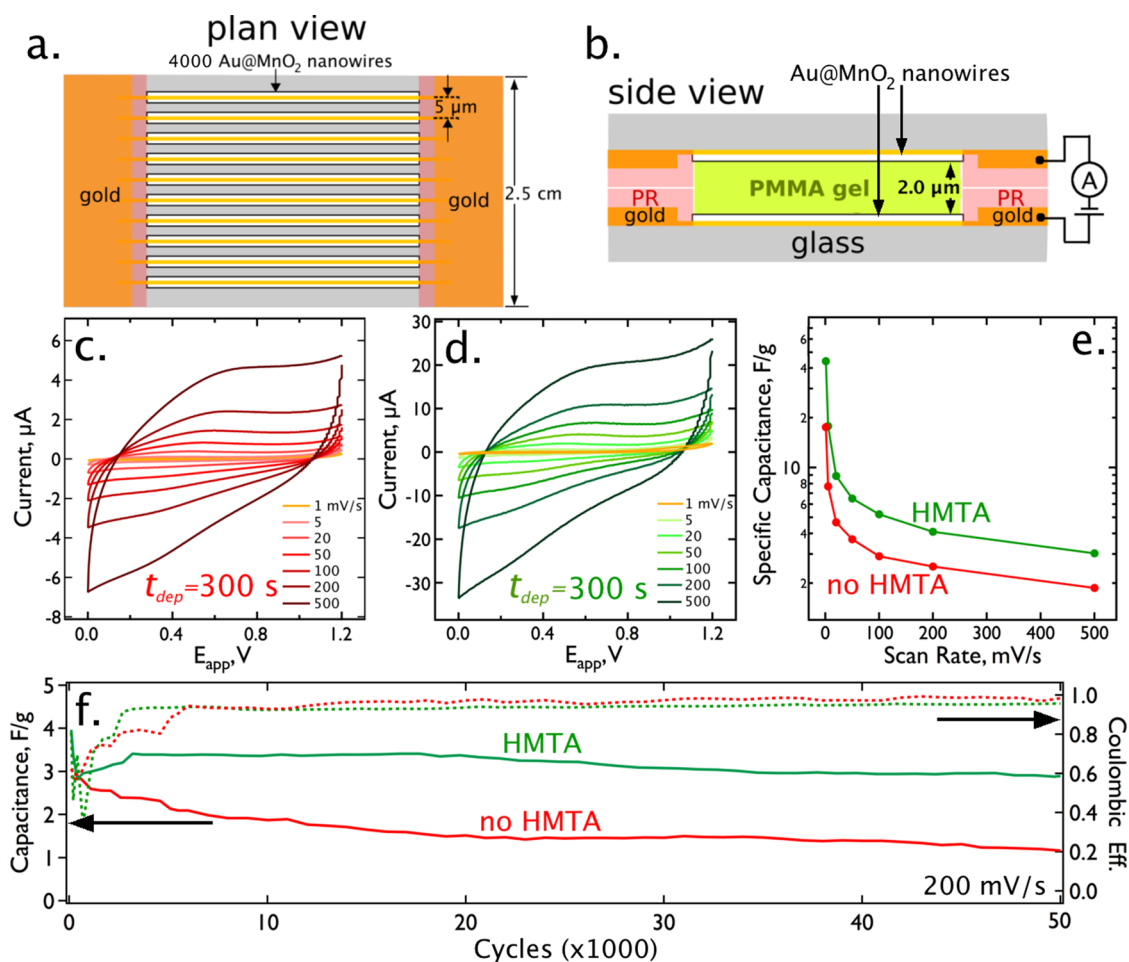
Figure 9. Cycle stability of C_{sp} for all-nanowire "sandwich" capacitors containing two 4000 Au@δ-MnO$_2$ (HMTA and no-HMTA) nanowire layers. (a,b) Schematic diagrams of the "sandwich" capacitor architecture.[32] (c,d) Cyclic voltammograms as a function of scan rate for HMTA and no-HMTA capacitors prepared using t_{dep} = 300 s. (e) C_{sp} versus scan rate for both capacitors. (f) C_{sp} (left axis) and Coulombic efficiency (right axis), measured at 200 mV/s, as a function of number of scans.

process because these nanowires are formed by electro-deposition entirely within the confines of a horizontal trench.

The conductance of solid δ-MnO$_2$ nanowires was measured in laboratory air by recording current versus potential ($I-V$) traces for an array of 200 nanowires across a 10 μm gap between two evaporated gold electrodes (Figure 8d−f). These $I-V$ traces were ohmic and clearly demonstrated a higher conductance for δ-MnO$_2$ prepared in the presence of HMTA relative to that in its absence, across all deposition times. This is immediately obvious from $I-V$ traces recorded at the same current sensitivity for HMTA and no-HMTA arrays (Figure 8d,f), which show much higher currents for the HMTA nanowires. HMTA increased the conductance of δ-MnO$_2$ nanowires by approximately 1 order of magnitude across all deposition times (Figure 8g). This factor is likely to contribute to the retention of C_{sp} by Au@δ-MnO$_2$ nanowires, particularly those with thick shells.

Finally, the improved performance of HMTA Au@δ-MnO$_2$ means little if its cycle stability is degraded. Recently,[7,32] we have demonstrated that no-HMTA Au@δ-MnO$_2$ nanowires cycled in a PMMA gel electrolyte, containing 1.0 M LiClO$_4$ in propylene carbonate, retain their specific capacity for 100,000 cycles or more.[7,32] This extraordinary level of cycle stability represents a new standard for nanowires. "Sandwich" capacitors were fabricated from two planar layers of Au@δ-MnO$_2$

nanowires (t_{dep} = 300 s), each layer containing 1800 nanowires (Figure 9a,b).[32] In these devices, the two nanowire arrays are separated by 5 μm of the PMMA gel electrolyte. Capacitors are hermetically sealed in a drybox and cycled in laboratory air. C_{sp} retention by Au@δ-MnO$_2$ nanowires was monitored for 50 000 cycles at 200 mV/s.

As already demonstrated in Figure 6, HMTA Au@δ-MnO$_2$ nanowires prepared with a 300 s MnO$_2$ deposition showed somewhat higher C_{sp} as compared with no-HMTA nanowires prepared the same way (4 F/g vs 2 F/g, Figure 9c−e). With cycling across 1.2 V at 200 mV/s, the initial C_{sp} is reduced somewhat for both types of nanowires but the HMTA versions retain a C_{sp} of 3 F/g after 50 000 cycles while the C_{sp} of no-HMTA nanowires decayed to ≈1.5 F/g over the same duration (Figure 9f). In future work, we are interested in understanding the origins of the superior retention of C_{sp} by the HMTA nanowires in these experiments.

■ CONCLUSIONS

We report investigations of the influence of the addition of the amine, HMTA, to the plating solution used to prepared the MnO$_2$ layer for Au@δ-MnO$_2$ core@shell nanowires. We find that HMTA changes the morphology of the MnO$_2$, increases the (001) interlayer spacing by ≈30%, and increases its electrical conductance by an order of magnitude. The net

influence of HMTA is to confer better retention of C_{sp} at high charge/discharge rates, and/or at high MnO_2 mass loadings. This is a large effect: C_{sp} for the thickest δ-MnO_2 shells, with t_{dep} = 500 s, were a factor of 15 times higher at 100 mV/s when HMTA was present in the plating solution.

While the rate performance of Au@δ-MnO_2 nanowires is certainly improved by HMTA, a considerable loss of C_{sp}—close to 50%—is still seen (Figure 7) for HMTA nanowires with the thickest MnO_2 shells (2.2 μm) relative to nanowires with the thinnest shells we examined (600 nm). This means that many Mn centers in the thickest MnO_2 shells are still not participating in charge storage on the time scale of these experiments.

■ AUTHOR INFORMATION

Corresponding Author
*E-mail: rmpenner@uci.edu.

ORCID
Rajen Dutta: 0000-0002-8572-2672
Il-Doo Kim: 0000-0002-9970-2218
Reginald M. Penner: 0000-0003-2831-3028

Notes
The authors declare no competing financial interest.

■ REFERENCES

(1) Wei, W.; Cui, X.; Chen, W.; Ivey, D. G. Manganese oxide-based materials as electrochemical supercapacitor electrodes. *Chem. Soc. Rev.* **2011**, *40*, 1697−1721.

(2) Yang, P.; Mai, W. Flexible solid-state electrochemical supercapacitors. *Nano Energy* **2014**, *8*, 274−290.

(3) Rolison, D. R.; Long, R. W.; Lytle, J. C.; Fischer, A. E.; Rhodes, C. P.; McEvoy, T. M.; Bourg, M. E.; Lubers, A. M. Multifunctional 3D nanoarchitectures for energy storage and conversion. *Chem. Soc. Rev.* **2009**, *38*, 226−252.

(4) Long, J. W.; Dunn, B.; Rolison, D. R.; White, H. S. Three-dimensional battery architectures. *Chem. Rev.* **2004**, *104*, 4463−4492.

(5) Yan, W.; Kim, J. Y.; Xing, W.; Donavan, K. C.; Ayvazian, T.; Penner, R. M. Lithographically patterned gold/manganese dioxide core/shell nanowires for high capacity, high rate, and high cyclability hybrid electrical energy storage. *Chem. Mater.* **2012**, *24*, 2382−2390.

(6) Yan, W.; Le Thai, M.; Dutta, R.; Li, X.; Xing, W.; Penner, R. M. A Lithographically Patterned Capacitor with Horizontal Nanowires of Length 2.5 mm. *ACS Appl. Mater. Interfaces* **2014**, *6*, 5018−5025.

(7) Le Thai, M.; Chandran, G. T.; Dutta, R. K.; Li, X.; Penner, R. M. 100k cycles and beyond: extraordinary cycle stability for MnO_2 nanowires imparted by a gel electrolyte. *ACS Energy Lett.* **2016**, *1*, 57−63.

(8) Zhang, Y.; Feng, H.; Wu, X.; Wang, L.; Zhang, A.; Xia, T.; Dong, H.; Li, X.; Zhang, L. Progress of electrochemical capacitor electrode materials: A review. *Int. J. Hydrogen Energy* **2009**, *34*, 4889−4899.

(9) Le, M. L.; Liu, Y.; Wang, H.; Dutta, R. K.; Yan, W.; Hemminger, J. C.; Wu, R. Q.; Penner, R. M. In-situ electrical conductivity of Li_xMnO_2 nanowires as a function of" x" and size. *Chem. Mater.* **2015**, *27*, 3494−3504.

(10) Liu, W.; Lu, C.; Wang, X.; Tay, R. Y.; Tay, K. High-performance microsupercapacitors based on two-dimensional graphene/manganese dioxide/silver nanowire ternary hybrid film. *ACS Nano* **2015**, *9*, 1528−1542.

(11) Lee, J. W.; Hall, A. S.; Kim, J.-D.; Mallouk, T. E. A facile and template-free hydrothermal synthesis of Mn_3O_4 nanorods on graphene sheets for supercapacitor electrodes with long cycle stability. *Chem. Mater.* **2012**, *24*, 1158−1164.

(12) He, Y.; Chen, W.; Li, X.; Zhang, Z.; Fu, J.; Zhao, C.; Xie, E. Freestanding three-dimensional graphene/MnO_2 composite networks as ultralight and flexible supercapacitor electrodes. *ACS Nano* **2013**, *7*, 174−182.

(13) Yan, J.; Fan, Z.; Wei, T.; Qian, W.; Zhang, M.; Wei, F. Fast and reversible surface redox reaction of graphene-MnO_2 composites as supercapacitor electrodes. *Carbon* **2010**, *48*, 3825−3833.

(14) Wu, Z.-S.; Ren, W.; Wang, D.-W.; Li, F.; Liu, B.; Cheng, H.-M. High-energy MnO_2 nanowire/graphene and graphene asymmetric electrochemical capacitors. *ACS Nano* **2010**, *4*, 5835−5842.

(15) Shi, P.; Li, L.; Hua, L.; Qian, Q.; Wang, P.; Zhou, J.; Sun, G.; Huang, W. Design of Amorphous Manganese Oxide@ Multi-Walled Carbon Nanotube Fiber for Robust Solid-State Supercapacitor. *ACS Nano* **2017**, *11*, 444−452.

(16) Gueon, D.; Moon, J. H. MnO_2 nanoflake-shelled carbon nanotube particles for high-performance supercapacitors. *ACS Sustainable Chem. Eng.* **2017**, *5*, 2445−2453.

(17) Li, Q.; Lu, X.-F.; Xu, H.; Tong, Y.-X.; Li, G.-R. Carbon/MnO_2 double-walled nanotube arrays with fast ion and electron transmission for high-performance supercapacitors. *ACS Appl. Mater. Interfaces* **2014**, *6*, 2726−2733.

(18) Fan, Z.; Yan, J.; Wei, T.; Zhi, L.; Ning, G.; Li, T.; Wei, F. Asymmetric supercapacitors based on graphene/MnO_2 and activated carbon nanofiber electrodes with High Power and Energy Density. *Adv. Funct. Mater.* **2011**, *21*, 2366−2375.

(19) Yang, S.-Y.; Chang, K.-H.; Tien, H.-W.; Lee, Y.-F.; Li, S.-M.; Wang, Y.-S.; Wang, J.-Y.; Ma, C.-C. M.; Hu, C.-C. Design and tailoring of a hierarchical graphene-carbon nanotube architecture for supercapacitors. *J. Mater. Chem.* **2011**, *21*, 2374−2380.

(20) Lin, H.; Li, L.; Ren, J.; Cai, Z.; Qiu, L.; Yang, Z.; Peng, H. Conducting polymer composite film incorporated with aligned carbon nanotubes for transparent, flexible and efficient supercapacitor. *Sci. Rep.* **2013**, *3*, 1353.

(21) Duay, J.; Gillette, E.; Liu, R.; Lee, S. B. Highly flexible pseudocapacitor based on freestanding heterogeneous MnO_2 conductive polymer nanowire arrays. *Phys. Chem. Chem. Phys.* **2012**, *14*, 3329−3337.

(22) Hou, Y.; Cheng, Y.; Hobson, T.; Liu, J. Design and synthesis of hierarchical MnO_2 nanospheres/carbon nanotubes/conducting polymer ternary composite for high performance electrochemical Electrode. *Nano Lett.* **2010**, *10*, 2727−2733.

(23) Kang, J.; Hirata, A.; Kang, L.; Zhang, X.; Hou, Y.; Chen, L.; Li, C.; Fujita, T.; Akagi, K.; Chen, M. Enhanced supercapacitor performance of MnO_2 by atomic doping. *Angew. Chem.* **2013**, *125*, 1708−1711.

(24) Li, W.; Liu, Q.; Sun, Y.; Sun, J.; Zou, R.; Li, G.; Hu, X.; Song, G.; Ma, G.; Yang, J.; et al. MnO_2 ultralong nanowires with better electrical conductivity and enhanced supercapacitor performances. *J. Mater. Chem.* **2012**, *22*, 14864−14867.

(25) Nakayama, M.; Tagashira, H.; Konishi, S.; Ogura, K. A direct electrochemical route to construct a polymer/manganese oxide layered structure. *Inorg. Chem.* **2004**, *43*, 8215−8217.

(26) Nakayama, M.; Hoyashita, R.; Komatsu, H.; Muneyama, E.; Shoda, K.; Kunishige, A. Immobilization of methylviologen between well-ordered multilayers of manganese oxide during their electrochemical assembly. *Langmuir* **2007**, *23*, 3462−3465.

(27) Nakayama, M.; Shamoto, M.; Kamimura, A. Surfactant-induced electrodeposition of layered manganese oxide with large interlayer space for catalytic oxidation of phenol. *Chem. Mater.* **2010**, *22*, 5887–5894.

(28) Nakayama, M.; Fujii, Y.; Fujimoto, K.; Yoshimoto, M.; Kaide, A.; Saeki, T.; Asada, H. Electrochemical synthesis of a nanohybrid film consisting of stacked graphene sheets and manganese oxide as oxygen evolution reaction catalyst. *RSC Adv.* **2016**, *6*, 23377–23382.

(29) Xiang, C.; Yang, Y.; Penner, R. M. Cheating the Diffraction Limit: Electrodeposited Nanowires Patterned by Photolithography. *Chem. Commun.* **2009**, 859–873.

(30) Xiang, C.; Kung, S.-C.; Taggart, D. K.; Yang, F.; Thompson, M. A.; Guell, A. G.; Yang, Y.; Penner, R. M. Lithographically patterned nanowire electrodeposition: a method for patterning electrically continuous metal nanowires on dielectrics. *ACS Nano* **2008**, *2*, 1939–1949.

(31) Menke, E. J.; Thompson, M. A.; Xiang, C.; Yang, L. C.; Penner, R. M. Lithographically patterned nanowire electrodeposition. *Nat. Mater.* **2006**, *5*, 914–919.

(32) Le Thai, M.; Qiao, S.; Dutta, R. K.; Jha, G.; Ogata, A.; Chandran, G. T.; Penner, R. M. Collateral advantages of a gel electrolyte for MnO_2 nanowire capacitors: higher voltage; reduced volume. *ACS Energy Lett.* **2017**, 1162–1169.

(33) Cooney, A. P.; Crampton, M. R.; Golding, P. The acid–base behaviour of hexamine and its N-acetyl derivatives. *J. Chem. Soc., Perkin Trans. 2* **1986**, 835–839.

(34) Dowding, J. M.; Das, S.; Kumar, A.; Dosani, T.; McCormack, R.; Gupta, A.; Sayle, T. X.; Sayle, D. C.; von Kalm, L.; Seal, S.; et al. Cellular interaction and toxicity depend on physicochemical properties and surface modification of redox-active nanomaterials. *ACS Nano* **2013**, *7*, 4855–4868.

(35) Dementjev, A.; De Graaf, A.; Van de Sanden, M.; Maslakov, K.; Naumkin, A.; Serov, A. X-ray photoelectron spectroscopy reference data for identification of the C 3 N 4 phase in carbon-nitrogen films. *Diamond Relat. Mater.* **2000**, *9*, 1904–1907.

(36) Mu, B.; Zhang, W.; Shao, S.; Wang, A. Glycol assisted synthesis of graphene–MnO_2–polyaniline ternary composites for high performance supercapacitor electrodes. *Phys. Chem. Chem. Phys.* **2014**, *16*, 7872–7880.